Synthetic Aperture FM-CW Radar Applied to the Detection of Objects Buried in Snowpack

Yoshio Yamaguchi, *Member, IEEE* , Masashi Mitsumoto, Masakazu Sengoku, *Member, IEEE*, and Takeo Abe, *Member, IEEE*

***Abstract*—This paper presents the principle of synthetic aperture frequency modulated continuous wave (FM–CW) radar and demonstrates the detection results of several objects buried in natural snowpack using the radar system. First, the synthetic aperture technique is explained with emphasis placed on showing that the Fourier transformed beat signal obtained by the FM–CW radar is equivalent to one kind of Fresnel hologram, which leads us to use SAR technique. Then a radar system operative in the microwave L-band is explored to detect objects buried in natural snowpack. Several detection results are presented demonstrating the potential capability of high resolution imaging in the azimuth direction, comparing with real aperture images.**

I. Introduction

In the field of imaging radars, the synthetic aperture technique has been successfully employed using pulse-radar systems for high-resolution areal mapping [1]–[5]. However, if the target is located very close to the radar antenna, say at a 1–2 meter distance, the pulse radar must have extremely high precision in the time domain, eg., nano (10^{-9}) to pico (10^{-12}) resolution to discriminate small range differences at such short distances [6], [7]. This high resolution and accuracy requirements in the time domain may impose severe restrictions in pulse radar design not to mention system costs, and these factors may pose a major disadvantage for its commercial use such as in shallow range detection of cables and pipes, etc. The FM–CW radars, however, utilize the continuous wave principle for which the range accuracy is determined by the frequency resolution which can be adjusted to a desired value. In addition, the FM–CW radar has a potential ability for measuring precise distances in the near range with less microwave power and simpler equipment, which makes its application convenient for shallow range detection. Our research goal is to develop an FM–CW imaging radar aimed at detecting and mapping objects buried in snowpack or in ground with relatively low losses.

If the synthetic aperture technique measurement capability is applied to the FM–CW radar, the radar will be promising in the shallow field detection and mapping such as in snowpack [8], [9] and in sandy ground. This paper extends the earlier work [8], [10], and presents the detection results of several objects in natural snowpack by an explored FM–CW radar in order to examine the performance of the system. In the following, the principle of synthetic aperture FM–CW radar is described showing that the beat spectrum obtained by the radar is equivalent to one kind of Fresnel hologram. The experimental results using natural snowpack are demonstrated to show the capability of this radar system for the precise detection comparing with the real aperture images.

Manuscript received August 7, 1992; revised July 18, 1993. This work was supported in part under a grant-in-aid for Scientific Research of the Ministry of Education, Japan.

Y. Yamaguchi, M. Mitsumoto, and M. Sengoku are with the Department of Information Engineering, Faculty of Engineering, Niigata University, Niigata-shi 950-21, Japan.

T. Abe is with the Department of Electronics Engineering, Chiba Institute of Technology, Narashino-shi, Chiba 275, Japan.

IEEE Log Number 9213370.

II. Principle of Synthetic Aperture FM–CW Radar

In this section, a brief description of basic principles necessary for introducing the synthetic aperture technique, based on the Fresnel hologram transformation approach, is given.

A. Principle of FM–CW Radar

The FM–CW radar basically measures a distance between antenna and an object by the beat frequency of transmitted signal and reflected signal from the object. The transmitting signal is usually swept linearly from $f_0 - \Delta f/2$ to $f_0 + \Delta f/2$ where f_0 is the center frequency. Fig. 1 shows the relation of frequency and time in the FM–CW radar. The transmitting signal can be expressed as a function of time as follows:

$$S_{tr}(t) = A\cos\left[2\pi\left(f_0 t + \frac{M}{2}t^2\right)\right] \tag{1}$$

where

A	amplitude,
f_0	center frequency in the frequency sweep,
t	time,
$M = \Delta f/\Delta t$	modulation rate,
Δf	sweep frequency width,
Δt	sweep time.

If an object whose reflection coefficient function is represented by

$$g = g(x_0, z_0) \quad (x_0, z_0)\text{: coordinate of the object} \tag{2}$$

is located at distance r from the transmitting antenna in a medium of permittivity ϵ_r, the scattered signal arriving at the receiving antenna is

$$S_{\text{rec}}(t) = gA'\cos\left[2\pi\left\{f_0(t-\tau) + \frac{M}{2}(t-\tau)^2\right\}\right] \tag{3}$$

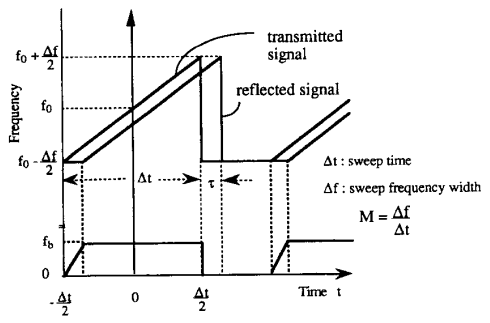

Fig. 1. Relation between time and frequency in FM–CW radar.

where

$$A' : \text{amplitude independent of } g;$$
$$\tau = \frac{2r}{c}\sqrt{\epsilon_r} : \text{time delay};$$
$$c = 3 \times 10^8 \text{ m/s}.$$

These two signals are mixed at a nonlinear device (mixer) producing the beat signal. After filtering out unnecessary frequency components, one can obtain the beat signal

$$S_b(t) = gAA' \cos\left[2\pi\left(f_0\tau + M\tau t - \frac{M}{2}\tau^2\right)\right]. \quad (4)$$

The coefficient $M\tau$ with respect to time t can be rewritten as

$$M\tau = \frac{2M\sqrt{\epsilon_r}}{c}r = \frac{2\sqrt{\epsilon_r}}{c}\frac{\Delta f}{\Delta t}r = f_b. \quad (5)$$

This value is the beat frequency proportional to distance r. Therefore the distance r is determined by obtaining f_b

$$r = \frac{c}{2\sqrt{\epsilon_r}}\frac{\Delta t}{\Delta f}f_b. \quad (6)$$

This is the well-known basic principle of the FM–CW radar. The parameters in our system are approximately

$$f_0 = 1.65 \times 10^9 \text{ Hz}, \tau \approx 10^{-8} \text{ s}, \Delta t = 5.2 \times 10^{-3} \text{ s}, M \approx 2 \times 10^{11},$$
$$f_0\tau = 16.5, M\tau \approx 2 \times 10^3, \tfrac{1}{2}M\tau^2 \approx 10^{-5}.$$

Therefore, the third term in the cosine argument of (4) can be neglected compared to the first and the second terms, which leads to

$$S_b(t) = gAA' \cos[2\pi(f_b t + f_0\tau)]. \quad (7)$$

In our system, f_b is determined via Fourier transform of (7). The Fourier transform with respect to time $(-(\Delta t/2) \le t \le \Delta t/2)$ for the positive frequency domain results in

$$S_b(f) = Bg \exp(j2\pi f_0\tau)\frac{\sin[\pi(f - f_b)\Delta t}{\pi(f - f_b)\Delta t} \quad (8)$$

with $B = AA'\Delta t/2$ being the amplitude. It should be noted that the Fourier transformed beat signal (8) does contain the phase term due to the time delay τ.

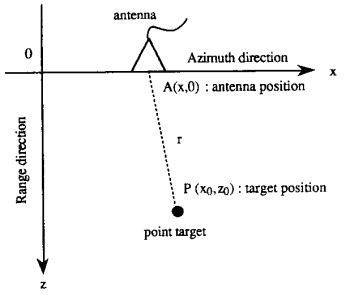

Fig. 2. Positions of antenna and point target.

B. Beat Spectrum and Hologram

The FM–CW radar scene is obtained by antenna scanning. The real aperture image is based on the amplitude information of (8) without the phase term [8]. However, the azimuth resolution of the real aperture image is reduced if the target is located far from the radar. In this section, we introduce the synthetic aperture technique for precise imaging in the azimuth direction. Let us assume that a reflection point exists in the Fresnel region as shown in Fig. 2. The distance r between the antenna and the target can be approximated as

$$r \approx z_0 + \frac{(x - x_0)^2}{2z_0}. \quad (9)$$

The time delay τ is therefore

$$\tau = \frac{2\sqrt{\epsilon_r}}{c}r \approx \frac{2\sqrt{\epsilon_r}}{c}\left[z_0 + \frac{(x - x_0)^2}{2z_0}\right]. \quad (10)$$

On the other hand, if we approximate $r \approx z_0$ in the evaluation of the sin function in (8), the beat frequency becomes

$$f_b \approx \frac{2\sqrt{\epsilon_r}}{c}\frac{\Delta f}{\Delta t}z_0. \quad (11)$$

Then, we find the following relations:

$$\pi(f - f_b)\Delta t \approx \frac{2\pi\sqrt{\epsilon_r}\Delta f}{c}(z - z_0) = \alpha(z - z_0),$$
$$\alpha = \frac{2\pi\sqrt{\epsilon_r}\Delta f}{c},$$
$$\frac{\sin[\pi(f - f_b)\Delta t}{\pi(f - f_b)\Delta t} = \frac{\sin[\alpha(z - z_0)]}{\alpha(z - z_0)}. \quad (12)$$

That is, the function in terms of the time can be transformed to the function in terms of the space variable z. Hence, the Fourier transformed beat spectrum (8) as a function of both time and space becomes a function of the space variable only. Now, we let the space variable function be $U(x, z)$

$$U(x,z) \equiv S_b(x,z,f) \approx S_b\left(x, z, \frac{\alpha}{\pi\Delta t}z\right) = S_b(x,z)$$
$$= Bg(x_0, z_0)\exp\left[j\frac{4\pi\sqrt{\epsilon_r}f_0}{c}\left\{z_0 + \frac{(x - x_0)^2}{2z_0}\right\}\right]$$
$$\cdot \frac{\sin[\alpha(z - z_0)]}{\alpha(z - z_0)}. \quad (13)$$

One can find that there exists a phase term due to the propagation path r. This phase term has been neglected in the standard real aperture FM–CW radars [8], [9]. For convenience, we divide (13) into three parts as follows:

1) the range function in the z direction

$$f(z-z_0)=\frac{\sin[\alpha(z-z_0)]}{\alpha(z-z_0)}=\mathrm{Sin}\,c[\alpha(z-z_0)] \tag{14}$$

2) the phase function with respect to the propagation path

$$h(x-x_0,z_0)=\exp\left[j\frac{4\pi\sqrt{\epsilon_r}f_0}{c}\left\{z_0+\frac{(x-x_0)^2}{2z_0}\right\}\right] \tag{15}$$

3) the object reflection coefficient distribution function $g=g(x_0,z_0)$. Therefore, (13) becomes

$$U(x,z)=Bf(z-z_0)\,g(x_0,z_0)\,h(x-x_0,z_0). \tag{16}$$

So far, we were concerned with a point target. If the target possesses two-dimensional areal distributions both in the azimuth direction x, and in the range direction z, then the beat spectrum (16) should be modified as

$$U(x,z)=B\int_0^{\infty}\int_{-\infty}^{\infty}f(z-z_0)\,g(x_0,z_0)\cdot h(x-x_0,z_0)\,dx_0\,dz_0. \tag{17}$$

This signal is recorded in our FM–CW radar system. One can see that this expression is of the convolution integral form and that this expression is equivalent to a Fresnel approximation to the Kirchhoff–Fresnel diffraction integral equation. The recorded pattern in the Kirchhoff–Fresnel diffraction is known as Fresnel hologram [11]. In our system, the recorded pattern is not an exact Kirchhoff–Fresnel diffracted one, however, we may consider it as one kind of Fresnel hologram because the recorded form is based on the integral equation of the same form.

C. Implementation of Synthetic Aperture Technique

At $z=z_0$, the range function becomes unity, which leads (17) to

$$U(x,z_0)=B\int_{-\infty}^{\infty}g(x_0,z_0)\,h(x_0-x,z_0)\,dx_0. \tag{18}$$

The object distribution function $g(x_0,z_0)$ can be obtained by an inverse convolution integral after multiplying the complex conjugated function h^* by U

$$g(x_0,z_0)=\int_{-(L/2)}^{L/2}U(x,z_0)\,h^*(x_0-x,z_0)\,dx. \tag{19}$$

L in (19) is the antenna-scan width in the azimuth direction, and symbol * denotes complex conjugation. This equation means that the object function at a certain depth z_0 can be recovered after successive measurement of U over an azimuth interval L using real aperture FM–CW radar. The object function at different depth can be obtained by changing z_0 and by calculating (19). This procedure would produce a high-resolution image in the azimuth direction in a radar scene. This equation establishes the basis for the synthetic aperture FM–CW radar principle. Therefore, it is possible to apply synthetic aperture technique to the FM–CW radar.

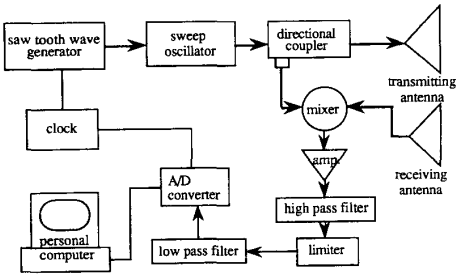

Fig. 3. Block diagram of FM–CW radar.

TABLE I
FM-CW RADAR SPECIFICATIONS

RF power	13 dBm
Frequency	1.1–2.2 GHz
Sweep time	5.2 ms
Antenna	Rectangular Horn
Aperture	40 × 32 cm
Sensitivity at mixer input	−42 dBm
Range resolution	5.5 cm in the air
Controller	32 bit personal computer
Scanning width	180 cm

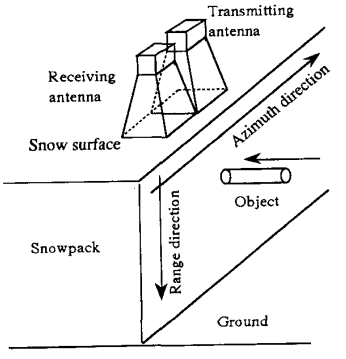

Fig. 4. Measurement scheme.

D. Signal Processing

The object reflection distribution function g (19) can be found via Fourier transformation [10], [12]

$$g(x_0,z_0)=\mathrm{FT}^{-1}[\mathrm{FT}(U)\cdot\mathrm{FT}(h^*)] \tag{20}$$

where FT: Fourier

FT^{-1}: inverse Fourier transform.

The radar image can be obtained by changing z_0 and using the corresponding value of the beat spectrum $U(x,z_0)$.

III. FIELD MEASUREMENTS

In this section, we present the experimental results obtained by an explored FM–CW radar system applied to the detection of objects buried in snowpack. The block diagram of the radar

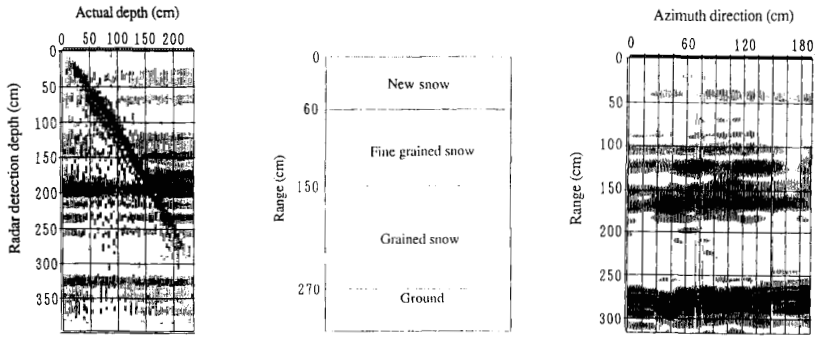

Fig. 5. The snowpack under the test on February 3, 1991. (a) Range detection result of a 5 × 100 cm plate. (b) Snow structure. (c) Snowpack image obtained by the radar.

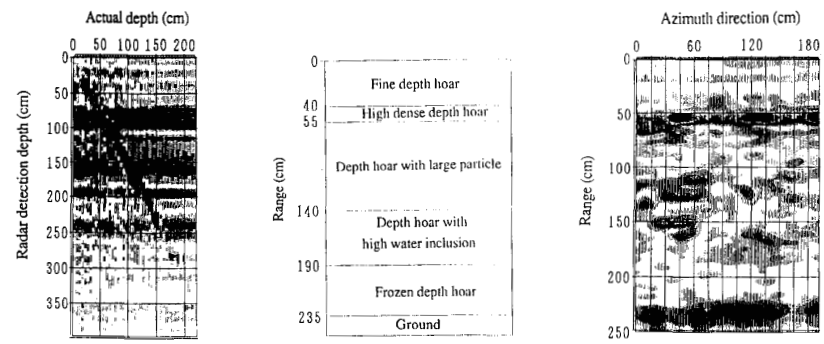

Fig. 6. The snowpack under the test on March 6, 1991. (a) Range detection result of a 5 × 100 cm plate. (b) Snow structure. (c) Snowpack image obtained by the radar.

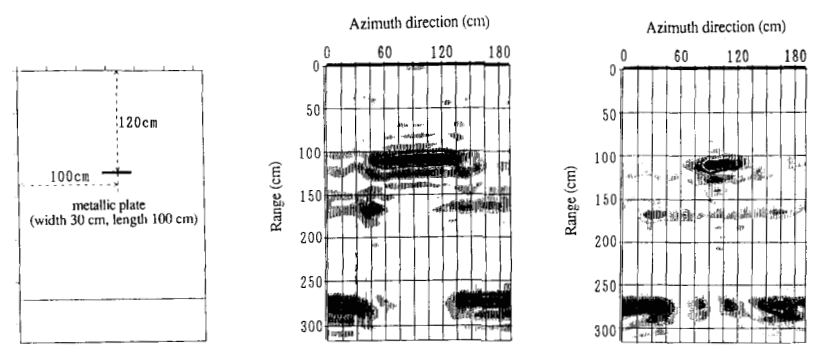

Fig. 7. Detection result of a 30 × 85 cm metallic plate on February 3, 1991. (a) Configuration. (b) Real aperture image. (c) Synthetic aperture image.

system is shown in Fig. 3. The radar specification are listed Table I. The measurements were carried out at Yamakoshi Village, Niigata Prefecture, Japan, on February 3, and on March 6, 1991. The snowpack was 270 cm deep and was rather dry on February 3, while it was 235 cm deep and was heavily wet on March 6. The measurement scheme is shown in Fig. 4.

A. Range Calibration

It is necessary to calibrate range r of (6) in the snowpack because the permittivity of the snowpack is unknown. The permittivity of snow varies with temperature, pressure by its own weight, time, and snow condition such as water inclusion, the size of snow particle [3], [13]. Thus, for the sake of range calibration, we first measured the target depth at which the

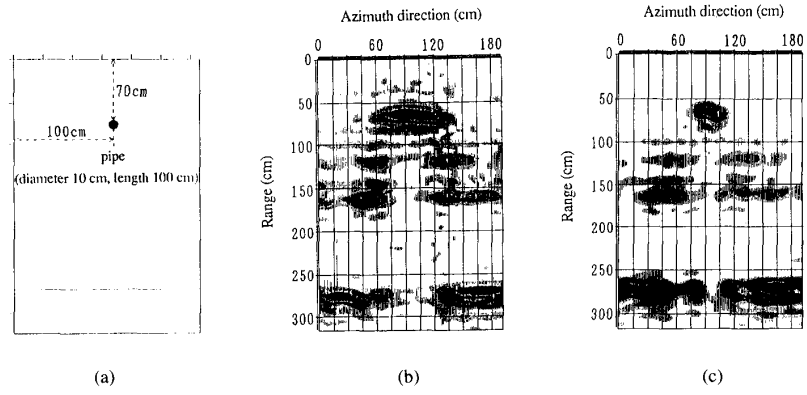

(a) (b) (c)

Fig. 8. Detection result of a 10 cmϕ × 100 cm metallic pipe on February 3, 1991. (a) Configuration. (b) Real aperture image. (c) Synthetic aperture image.

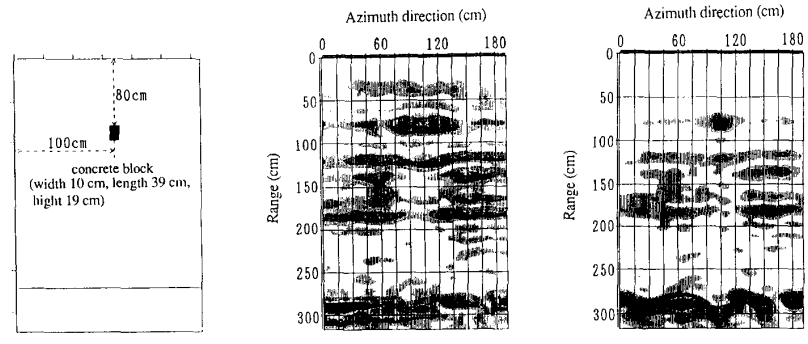

(a) (b) (c)

Fig. 9. Detection result of a 10 × 39 × 19 cm concrete block on February 3, 1991. (a) Configuration. (b) Real aperture image. (c) Synthetic aperture image.

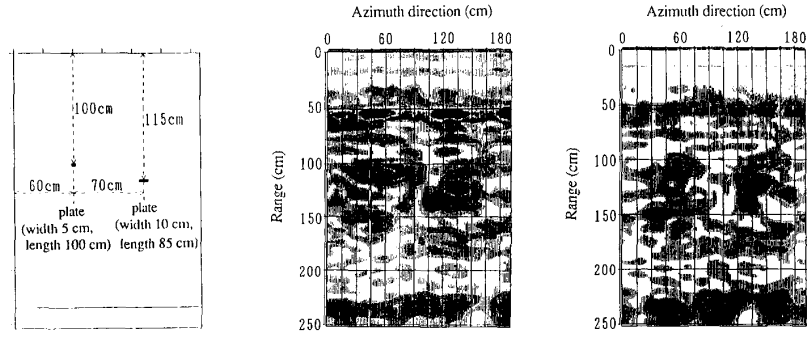

(a) (b) (c)

Fig. 10. Detection result of 5 × 100 cm and 10 × 85 cm metallic plates on March 6, 1991. (a) Configuration. (b) Real aperture image. (c) Synthetic aperture image.

radar could identify in the snowpack using a metallic plate of 100 cm long, 5 cm wide, and 3 mm thick. The plate was inserted horizontally into the snowpack at 5 cm intervals in the range direction, i.e., in the vertical direction so as to match the polarization direction of the transmitted wave. The detection results are shown in Fig. 5(a) and Fig. 6(a). In both figures, the vertical axes represent the depth measured by the radar, while the horizontal axes represent the actual depth. Nine uniform quasi-gray scales have been used to cover the normalized magnitude in the Fourier-transformed domain with black indicating strong reflection. Fig. 5 corresponds to the snowpack on February 3, while Fig. 6 corresponds to that on March 6. Once the target depth by the radar is obtained, it is possible to determine the average permittivity of the snowpack and calibrate the range according to (6). The average snow permittivities were found to be 1.6 and 2.5 from the slope of

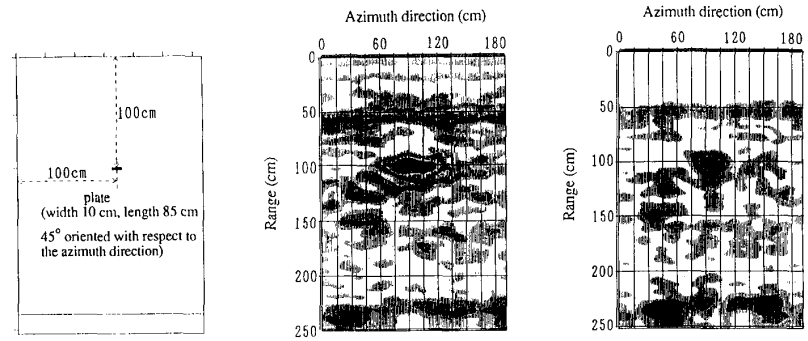

(a) (b) (c)

Fig. 11. Detection result of a 5 × 100 cm metallic plates which oriented 45 degrees with respect to scanning direction. (a) Configuration. (b) Real aperture image. (c) Synthetic aperture image.

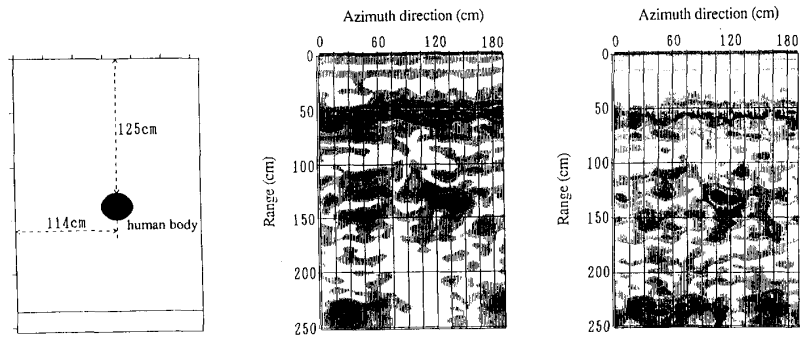

(a) (b) (c)

Fig. 12. Detection of result of human body detection on March 6, 1991. (a) Configuration. (b) Real aperture image. (c) Synthetic aperture image.

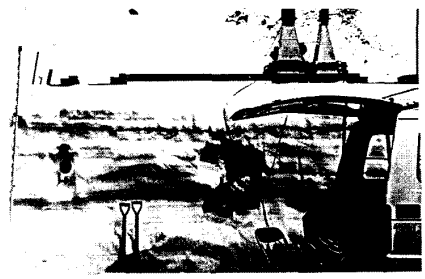

Fig. 13. Experimental scene of human body detection.

Fig. 5(a) and Fig. 6(a), respectively. These figures also show the maximum detection range of the radar in the snowpack. It was possible to detect the metallic plate at 250 cm deep and even the ground surface of 270 cm on February 3 in Fig. 5(a). For the case of March 6 in Fig. 6(a), the maximum range was approximately 150 cm.

B. Snowpack

Figs. 5(b) and 6(b) display the snowpack structures which consisted of multiple stratified snow layers. For the case of February 3 in Fig. 5(b), the snowpack was physically homogeneous in the horizontal direction from the eye observation. The snow temperature was $-0.1°C$ throughout the snowpack. The snow density was 0.35 g/cm^3 at the upper portion of the new snow layer and it gradually increased to be 0.45 g/cm ^{3} at the grained snow layer. This snowpack structure was measured by scanning the radar antennas along the azimuth direction (in the horizontal direction) preceding the object detection. The real aperture image of the snowpack is shown in Fig. 5(c). The range in this figure is calibrated according to the permittivity (= 1.6) of the snowpack. From Fig. 5(c), one can see that the natural snowpack is electrically homogeneous in the horizontal direction, although one can recognize clutter due to the snow layer boundaries in the vertical direction.

On the other hand, for the case of March 6 in Fig. 6(b), the snowpack had undergone melting cycles repeatedly coupled with rainfall, the snow condition was very adverse for radar detection. Since the snowpack was heavily wet, the snow density from the surface to the depth of 190 cm was 0.43 g/cm^3 and was 0.53 g/cm^3 at the bottom. Especially, a snow layer at about 50 cm deep contained water heavily (more than 14.5% of water inclusion, one could see water layer at the measurement). This snow layer degraded the performance of the radar. The temperature was $-0.1°C$ throughout the snowpack. The real

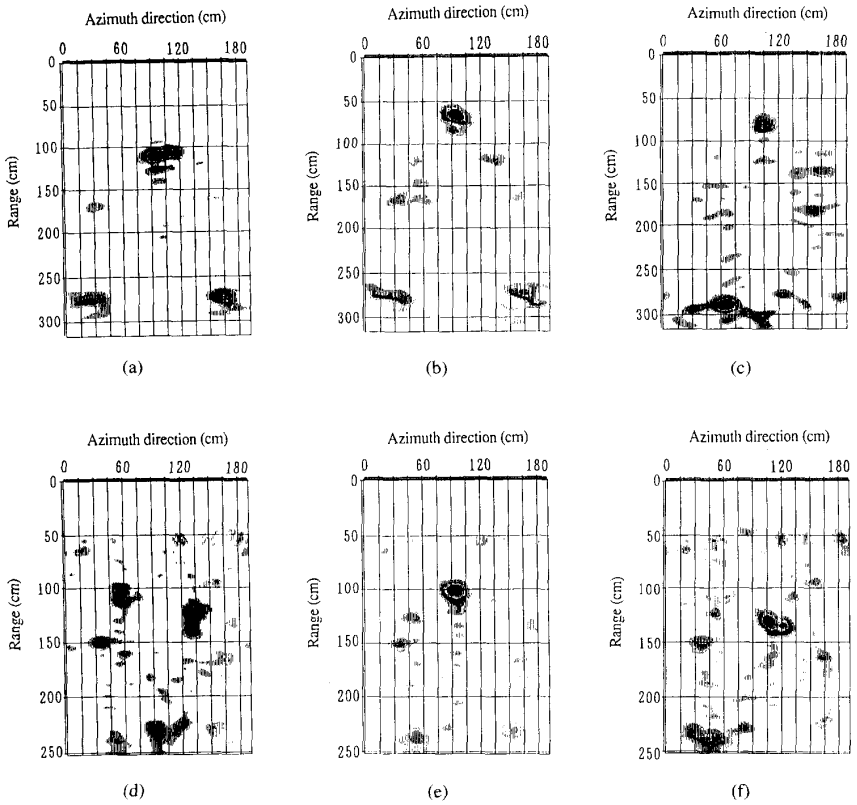

Fig. 14. Enhanced images of Figs. 6–11(c) by an averaging and subtracting method (a) A metallic plate. (b) A metallic pipe. (c) A concrete block. (d) Two plates. (e) A 45 degree oriented plate. (f) Human body.

aperture image of the snowpack is shown in Fig. 6(c) where the range is calibrated according to the permittivity (= 2.5) of the snowpack. The internal structure was quite complex due to melting which caused irregular clutter as seen in Fig. 6(c).

C. Object Detection

Both the transmitting and receiving antennas were scanned along a rail in the azimuth (horizontal) direction at a 1.5 cm interval by hand on the snow surface to detect targets embedded in the snowpacks. The scanning length was 192 cm, which produced 128 sampling points in the azimuth direction. The data acquisition time for obtaining one beat spectrum was 20 msec., but it took 20 min. for one radar image due to hand manipulation of the antenna scan. The experimental configurations and the detection results are illustrated in Figs. 7–12. In these figures, (a) shows the target position in the snowpack, (b) shows the real aperture image and (c) shows the synthetic aperture image based on (19). These images typically consist of 128 × 300 pixels (which are dependent of range). The synthetic aperture processing time required for one image is approximately 10 min. by a personal computer (80386 + 80387, 20 MHz clock).

The detection results obtained on February 3 are shown in Figs. 7–9. Fig. 7 shows the detection result of metallic plate buried at 120 cm deep from the snow surface. The plate was inserted horizontally so as to match the polarization direction of the radar wave. It is seen in Fig. 7(b), the strongest reflection comes from the region where the plate is inserted, and the second strongest reflection appears around the ground surface. The detection image is widespread in the azimuth direction due to real aperture image, however, it is focused by the synthetic aperture technique as shown in Fig. 7(c). This synthetic aperture image provides the accurate position information of the plate in the snowpack. Fig. 8 shows the detection results of a metallic pipe of 10 cmϕ buried 70 cm deep in the snow. Although the reflection magnitude of the pipe was weaker than that of the plate and the clutter in the snowpack appeared relatively strong in the image, it was possible to map the pipe accurately (Fig. 8(c)).

Next, we buried a concrete block (10 cm wide, 39 cm long, 19 cm high) at the depth of 80 cm (Fig. 9(a)). This nonmetallic target reflects a weak scattered wave, of which strength is comparable to the clutter level (Fig. 9(b)). The synthetic aperture image in Fig. 9(c) suppresses the clutter in Fig. 9(b) and provides the target information.

The results obtained on March 6 are shown in Figs. 10–12. Fig. 10 shows the detection result of two metallic plates. One of the plates was 5 cm wide and 100 cm long and was inserted at the depth of 100 cm, another plate was 10 cm wide and 85 cm long and inserted at the depth of 115 cm (Fig. 10(a)). Severe clutter degraded the real aperture detection

image of Fig. 10(b), however, the positioning of these targets might be recognized by the synthetic aperture technique (Fig. 10(c)) which enhanced the target location. The validity of the synthetic aperture technique is not so apparent compared to that in the snowpack on February 3 due to the attenuation of the wave in the snowpack and due to the clutter because the sounding capabilities are reduced by adverse snow conditions.

Fig. 11 shows the other result of metallic plate. The plate was inserted horizontally, but the direction was oriented 45° with respect to the direction of polarization of the radar wave. This setup is assumed on the fact that the buried object is not always parallel to the direction of polarization in the actual detection situation. Fig. 11(b) provides the real aperture image for which we can recognize the target. The wide spread target image is compressed in the azimuth direction by the synthetic aperture technique.

Next, we dug a small horizontal hole where a person could be buried. The upper rim of the hole was 125 cm deep from the surface. One of us became a snow avalanche victim model. He lay horizontally with his body parallel to the polarization direction of the wave. Fig. 13 shows the experimental scene. The detection result is shown in Fig. 12. The boundary of him was not so clear due to the clutter in the image of Fig. 12(b) even though the victim was detected. On the other hand, the synthetic aperture image Fig. 12(c) provided the boundary distinctively and gave an accurate position of him.

So far, the real and the synthetic aperture images are presented and compared to show the difference in the detection results. The synthetic aperture images provided clear and accurate boundaries of the targets even though the targets were buried in inhomogeneous medium. However, there still remains clutter in the synthetic aperture image. The reduction of noise and clutter is important for mapping the target. Since the usual snowpack consists of horizontal snow layers, which in turn, makes us carry out some processing to retrieve information from this characteristic structure [8]. That is, 1) we first average the value of column data at a certain depth in the azimuth direction (averaged value = A), 2) then transform each pixel data B at that depth in a way such that B − A, 3) repeat the same procedure for each depth, and 4) renormalize the scene. If the value B − A becomes negative, the value is set to be zero. This simple averaging and subtracting technique renders the synthetic images of Fig. 7–11 very clear, suppressing clutter, as shown in Fig. 14. In all cases, clutter due to the horizontal snow layers are suppressed and the final image quality is considerably increased.

IV. Conclusion

In this paper, we demonstrated the fundamental result of synthetic aperture FM–CW radar applied to the detection of objects in natural snowpack. By implementation of the synthetic aperture technique, it was possible for the FM–CW radar to obtain images with high resolution in the azimuth direction in the snowpack. Although the synthetic aperture performance is restricted by many factors such as the wave attenuation and clutter, this technique provided clear boundary of the target position in the snowpack. Finally, an averaging and subtracting processing technique is employed to make the synthetic aperture image clear, suppressing the clutter which is characteristic to the natural snowpack structure. From the experiment, this imaging FM–CW radar seems to have a potential ability to map objects embedded in a lossy medium.

References

[1] D. R. Wehner, *High Resolution Radar.* Dedham, MA: Artech, 1987.
[2] J. P. Fitch, *Synthetic Aperture Radar.* New York: Springer-Verlag, 1988.
[3] F. T. Ulaby, R. K. Moore, and A. K. Fung, *Microwave Remote Sensing—Active and Passive, Vols I–III.* Dedham, MA: Artech, 1986.
[4] T. Yoshida, *Radar Technique.* IEICE Japan, 1985.
[5] A. B. Kostinski, B. D. James, and W.-M. Boerner, "Polarimetric matched filter for coherent imaging," *Can. J. Phys.*, vol. 66, pp. 871–877, 1988.
[6] N. Osumi and K. Ueno, "Microwave holographic image of underground objects," *IEEE Trans. Antennas Propagat.*, vol. AP-33, no. 2, pp. 152–159, Feb. 1985.
[7] Y. Michiguchi, K. Hiramoto, M. Nishi, T. Ohtaki, and M. Okada, "Advanced subsurface radar system for imaging of buried pipes," *IEEE Trans. Geosci. Remote Sens.*, vol. 26, no. 6, pp. 733–740, Nov. 1988.
[8] Y. Yamaguchi, A. Kawakami, Y. Maruyama, M. Sengoku, and T. Abe, "Detection of objects buried in wet snowpack by an FM–CW radar," *IEEE Trans. Geosci. Remote Sens.*, vol. 29, no. 2, pp. 201–208, Mar. 1991.
[9] Y. Yamaguchi, M. Mitsumoto, M. Sengoku, and T. Abe, "Human body detection in wet snowpack by an FM–CW radar," *IEEE Trans. Geosci. Remote Sens.*, vol. 30, no. 1, pp. 186–189, Jan. 1992.
[10] Y. Yamaguchi, M. Mitsumoto, A. Kawakami, M. Sengoku, and T. Abe, "Detection of objects by synthetic aperture FM–CW radar," *Trans. IEICE Japan,* vol. J74-B-II, pp. 413–420, July 1991.
[11] E. Yamashita, *Introduction to Electromagnetic Wave Engineering.* Sangyo Tosho, Japan, 1980.
[12] Y. Aoki, *Wave Signal Processing.* Morikitasyuppan, Japan, 1986.
[13] M. Halikainen, F. T. Ulaby and M. Abdelrazik, "Dielectric properties of snow in the 3 to 37 GHz range," *IEEE Trans. Antennas Propagat.*, vol. AP-34, pp. 1329–1340, Nov. 1986.

Yoshio Yamaguchi, for a photograph and biography, please see p. 208 of March 1991 issue of this TRANSACTIONS.

Masashi Mitsumoto received the B.E. degree in information engineering from Niigata University, Japan, in 1990. He is now a graduate student in Niigata University where he is engaged in microwave imaging using FM–CW radar.

He is an Associate Member of the Institute of Electronic, Information and Communication Engineers (IEICE) of Japan.

Masakazu Sengoku, for a photograph and biography, please see p. 208 of March 1991 issue of this TRANSACTIONS.

Takeo Abe, for a photograph and biography, please see p. 208 of March 1991 issue of this TRANSACTIONS.